

PhD.Student, Mihai-Alexandru Grigoroscuta

Boron and rare earth based materials for energy applications



POLITEHNICA UNIVERSITY OF BUCHAREST

Faculty of Science and Materials Engineering

Department of Metallic Materials Science, Physical Metallurgy

PhD THESIS

Materiale pe bază de boruri și pământuri rare pentru aplicații energetice

Boron and rare earth based materials for energy applications

Author:

Mihai-Alexandru GRIGOROȘCUȚĂ

Coordinator:

Mihai Ovidiu COJOCARU

Bucharest
2021

KEYWORDS

Superconductors: magnesium boride (MgB_2), magnetic field texture, bulks, Spark Plasma Sintering (SPS), magnetic and electric measurements (SQUID, PPMS), superconductor tapes, superconductor magnets, magnetic shielding, magnetic storage.

Luminiscent materials: rare earth Yb and Er ions, CeO_2 , thin films, optical properties determinations (diffuse reflectance, photoluminescence), power conversion efficiency (*PCE*), silicon solar cell.

Structural materials: Al-B-C system, $\text{AlB}_{24}\text{C}_4$ phase, static and dynamic mechanical properties, Split-Hopkinson Pressure Bar (SHPB) technique.

TABLE OF CONTENTS	
CH. 1. GENERAL ASPECTS. ENERGY CONSUMPTION, PRODUCTION AND GENERATION. COMPOSITE MATERIALS FOR ENERGY APPLICATIONS AND THEIR EFFICIENCY	
1.1. Energy production and consumption	1
1.2. Renewable energies and applications of interest	
1.2.1. Solar energy	1
1.2.2. Wind energy	2
1.2.3. Hydro energy	3
1.2.4. Nuclear energy	3
1.3. Materials for energy and their efficiency	
1.3.1. Superconductor materials	3
1.3.2. Luminescent materials	3
1.3.3. Structural materials	3
CH. 2. PROCESSING TECHNIQUES AND METHODS OF INVESTIGATION OF THE COMPOSITE MATERIALS	
2.1. Processing techniques of composite materials	
2.1.1. Slipcasting under 12 T magnetic field	4
2.1.2. Spark Plasma Sintering (SPS)	5
2.1.3. Pulsed Laser Deposition (PLD)	5
2.2. Microstructural and compositional properties	
2.2.1. X-ray diffraction (XRD)	5
2.2.2. Relative density determination by assesment of the SPS contraction curves	5
2.2.3. Scanning Electron Microscopy (SEM)	5
2.2.4. Atomic Force Microscopy (AFM)	5
2.3. Superconducting properties and measurement methods	
2.3.1. Magnetic measurements (VSM, SQUID, PPMS)	5
2.3.2. Electric measurements (PPMS)	5
2.4. Luminescent spectroscopy and power conversion measurements	
2.4.1. Diffuse reflectance and photoluminiscence measurements	5
2.4.2. Power conversion efficiency (PCE)	5
2.5. Structural materials properties	
2.5.1. Hardness determination	5
2.5.2. Dynamic impact properties by Split-Hopkinson Pressure Bar (SHPB) measurements	5

CH. 3. EXPERIMENTAL RESULTS AND DISCUSSION. DIFFERENT TYPES OF COMPOSITE MATERIALS FOR ENERGY APPLICATIONS.

3.1. Superconducting materials, storage and transportation of energy

3.1.1. Doped MgB₂ for the improvements of superconductor and mechanical properties **5**

3.1.2. MgB₂ for magnetic energy storage, magnets applications **6**

3.1.3. MgB₂ tapes for efficient electrical current transportation **7**

3.1.4. Shaped MgB₂ for electromagnetic shielding applications **8**

3.1.5. Magnetically textured MgB₂ **9**

3.2. Rare earth luminescent materials for solar cells

3.2.1. Yb/Er doped CeO₂ thin films for spectral conversion in silicon solar cells **10**

3.3. Structural materials

3.3.1. Al-B-C composites for mechanical protection in nuclear energy applications **11**

CONCLUSIONS **13**

PERSONAL CONTRIBUTIONS - ORIGINALITY **14**

PUBLISHED PAPERS **16**

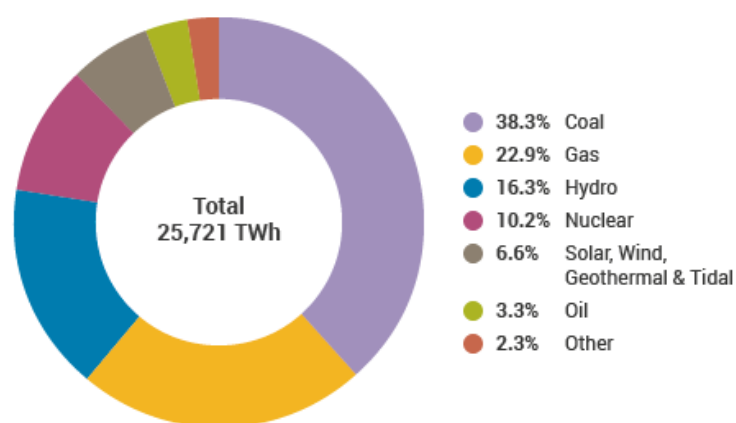
REFERENCES **18**

Boron and rare earth based materials for energy applications

The thesis presents three types of boron and rare earths materials that can be used for energy applications. It is composed of 3 chapters that show the importance of development of new composite materials, such as *superconductors*, *luminiscent materials* and *structural materials*.

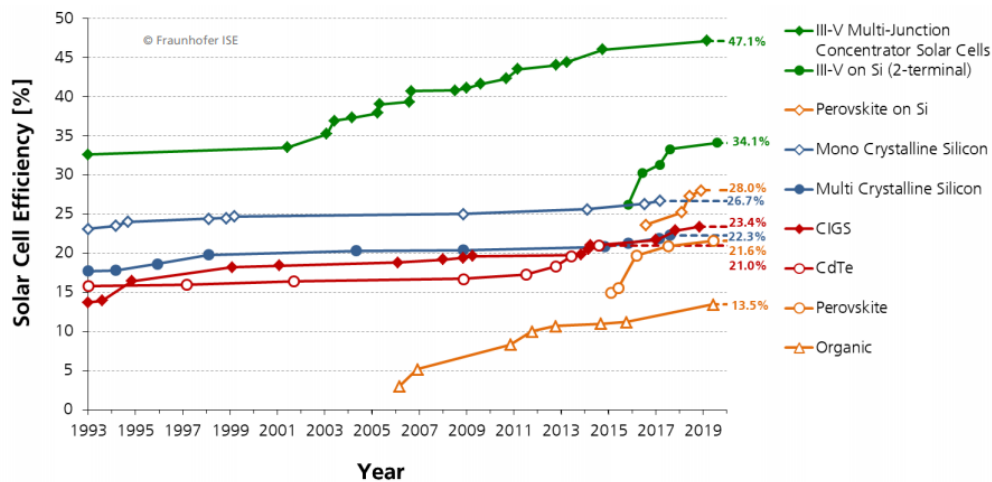
Chapter 1 presents the state of the art in global production of energy. The intense use of conventional burnable resources (coal, natural gas, petrol) for production and consumption of energy pose different environmental economic and social problems [1]. In 2015, *The Paris Agreement* was signed by 200 states and established a limit of +1,5 °C for global warming. To achieve this goal it is necessary to use renewable resources with limited or no impact on the environment [4]. Among these resources, the most relevant for global consumption are solar energy, wind energy, hidro energy, and nuclear energy.

World Electricity Production by Source 2017

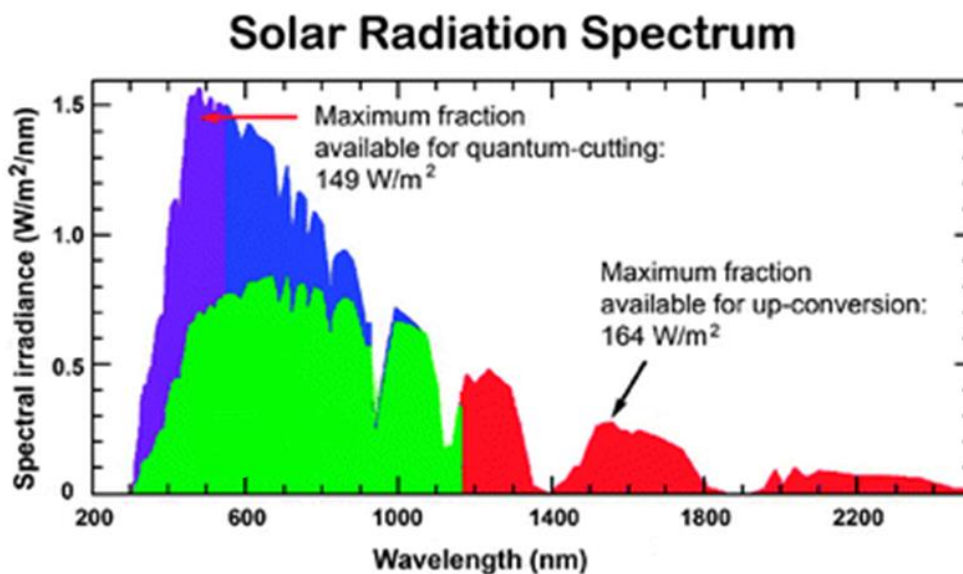


Source: IEA Electricity Information 2019

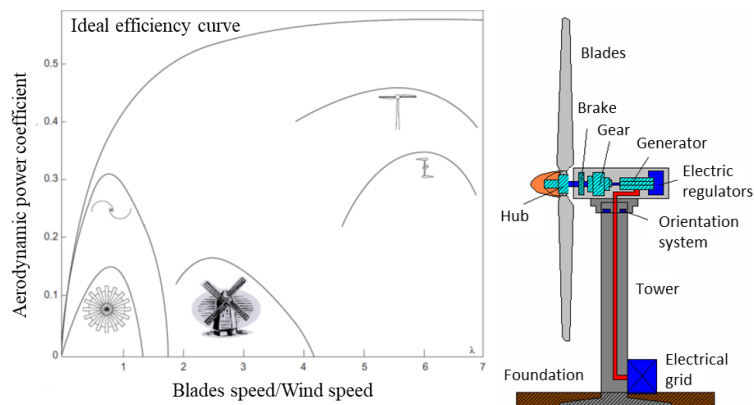
Section 1.2.1. Solar energy can be converted to heat or electricity with devices known as solar cells. For different materials, the efficiency of power conversion can reach about 30 % (eg. CdTe 21 %, CIGS 23,4 %). The most common type of solar cells use semiconducting silicon. This material is abundant and cheap. The silicon based solar cells have the conversion efficiency between 22 – 26,7 %.



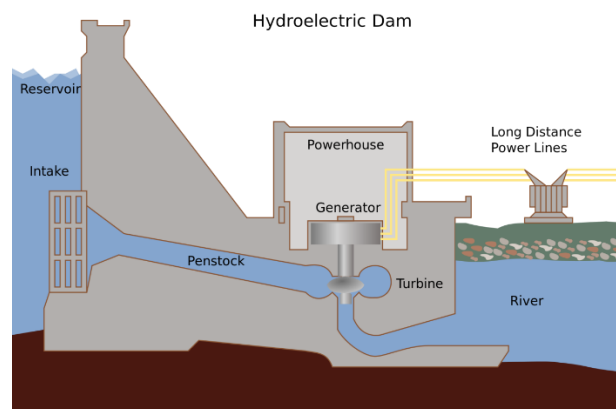
To further improve the efficiency of solar cells, research of new materials in this field is important. One way to achieve this goal is to use thin films made of special *luminescent materials*. These layers can help to convert the unused part of the solar spectrum by a silicon solar cell to the useful region (down-conversion, up conversion) [8].



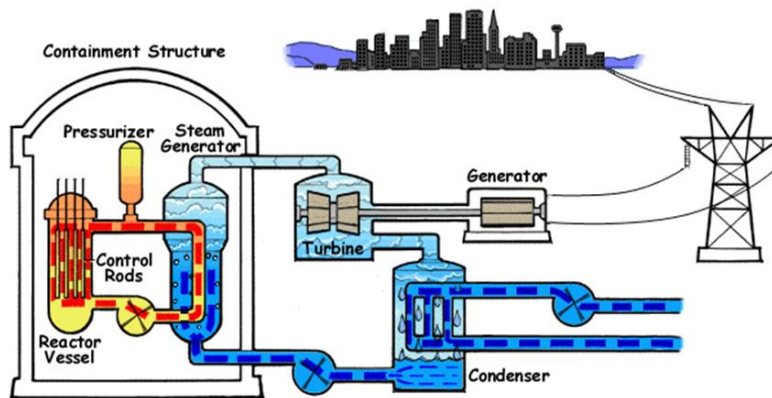
Section 1.2.2. The wind energy can use the so called wind turbines and can have a maximum efficiency of 59,3 % [10]. Energy wind mills are composed of a structural tower, an electrical turbine, and the moving blades. For the fabrication of the turbines, materials such as *superconductors* can be used to limit the electrical losses and reduce noise.



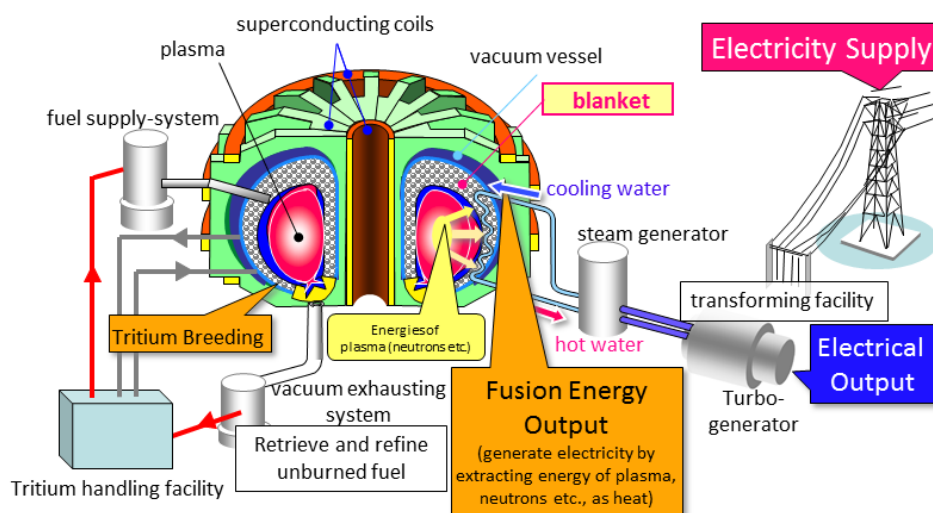
Section 1.2.3. The hidro energy is the most common form of renewable energy. Hydropower plants can achieve over 75% efficiency and produce up to 500 MW of electricity. One great advantage of these plants is their long lasting life (40 to 80 years) [12]. Materials requirement in this field is focused on water corrosion resistance and electrical current transportation (turbine, power transformers, transport cables). As for the wind energy, construction of the turbines generator can use *superconductors*.



Section 1.2.4 Nuclear energy is a form of energy obtained by fission and fusion processes. Today, nuclear power plants use nuclear fission. The splitting of atoms produce neutrons and other nuclear particles that can generate extreme heat. The heat is mainly used to power up a gas (water vapour) turbine and produce electricity. The result of this process is also production of nuclear waste. Therefore, for security reasons, *special materials* are necessary showing *low neutron cross section, high durability, and resistance to impact and high temperatures* [14]. Boron based materials are important in this field.



The use of fusion process gives the opportunity to generate electricity without nuclear waste. One of the most important experiments is ITER. The reactor constructed and tested within this research project managed to produce 10 times the energy used to power it. This technology is based on the use of a high and homogenous magnetic field to confine a plasma. The essential materials to produce high magnetic fields are the *superconductors*. Other special materials are needed for fusion reactors.

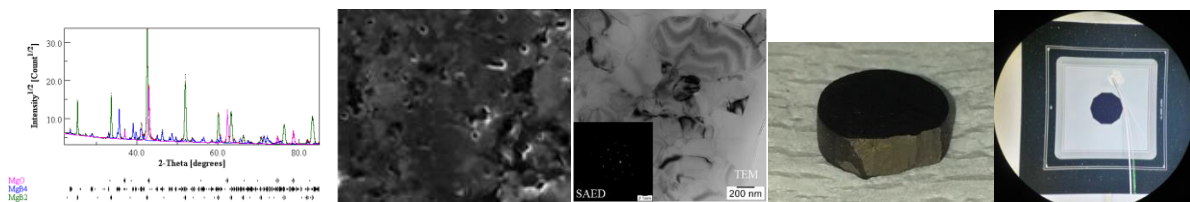


The aim of this work is to study MgB_2 composite bulk superconductors, Yb/Er CeO_2 rare earth thin film luminescent materials and Al-B-C structural composites for energy applications.

Chapter 1 also presents the specific properties of superconductors, luminescent materials for conversion and structural materials. Definitions, state of the art in research of these materials, key functional properties important for their quality assesment and possible practical applications are addressed.

Chapter 2 describes the methods used to process and characterize the previously mentioned materials. The Spark Plasma Sintering technique was used to produce MgB_2 (bulks and tapes) and Al-B-C (bulks) composites. The luminescent thin films were grown by Pulsed Laser

Deposition. The structural and microstructural aspects were investigated by X-ray Diffraction, Scanning Electron Microscopy, Transmission Electron Microscopy and Atomic Force Microscopy. The magnetic and electric measurements of MgB₂ bulks and tapes were performed with a Superconducting Quantum Interference Device and a Physical Properties Measurement System. The optical properties were investigated by Diffuse Reflectance Spectroscopy and Photoluminescence measurements. The conversion efficiency of the solar cells was estimated considering the current-voltage experimental data measured in a solar simulator. The mechanical properties were determined with a Vickers microindentation tester and the Split-Hopkinson Pressure Bar equipment.

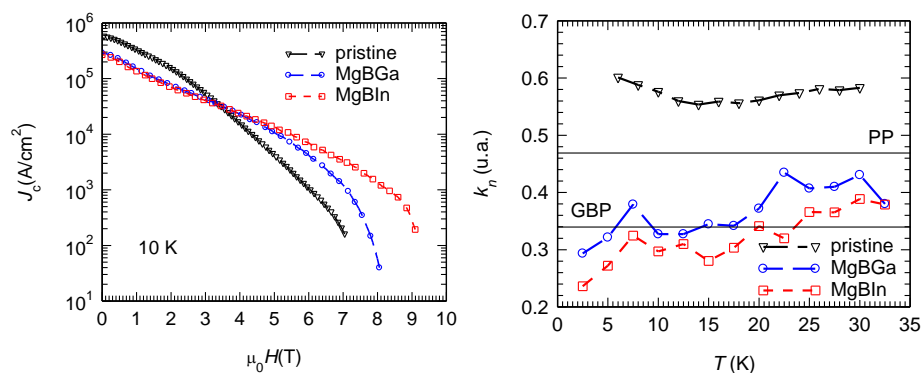


Examples of XRD diffraction, SEM, TEM, a MgB₂ sintered sample and a silicon solar cell.

Chapter 3 presents the experimental results and the interpretation of the measurements for the MgB₂ composite bulks and tapes, the luminescent thin films, and the Al-B-C composite bulks.

In Section 3.1.1, C₁₅H₂₁InO₆ and C₁₅H₂₁GaO₆ (A.) [A1], Ho₂O₃ and metallic Te (B.) [A2] and SiC and metallic Te (C.) [A3] added MgB₂ bulks are obtained and investigated.

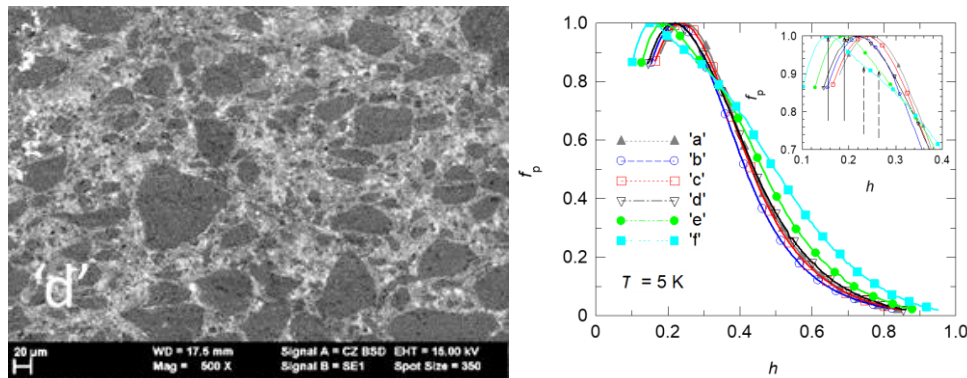
A. The dense bulk samples with addition of C₁₅H₂₁InO₆ and C₁₅H₂₁GaO₆ showed improvements of critical current density J_c at high magnetic fields for temperatures below 25 K. Introduction of additives modifies the microstructure and the level of carbon substitution for boron in the crystal structure of MgB₂. These details improve the vortex pinning especially the grain boundary pinning (GBP) [23, 24] and thus the critical current density is enhanced.



Critical current density J_c and k_n coefficient for the MgB₂ sintered samples. $k_n \geq 0,47$ for point pinning (PP) and $k_n \geq 0,34$ for grain boundary pinning (GBP) [23, 24].

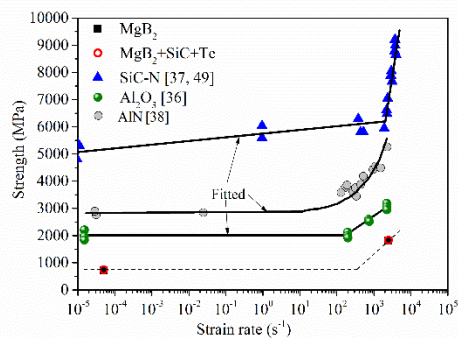
B. Dense bulk samples with addition of Ho₂O₃ and metallic Te, with starting composition (MgB₂)_{0.99}(Te_x(HoO_{1.5})_y)_{0.01}, with $x/y = 2,7, 1,32, 0,67, 0,45$ and $0,33$ were fabricated by Spark

Plasma Sintering. The optimal microstructure with best superconducting properties was obtained for $x/y = 0,67$ (sample 'd'). The shape of the reduced pinning force (f_p) curve shows a shoulder. The shoulder separation is stronger for $x/y = 0,67$ (when $x/y \leq 0,67$).



SEM image (in backscattering mode) obtained for sample 'd' ($x/y = 0,67$). The white color indicates the presence of heavy element (Ho). The reduced force pinning f_p vs. reduced field h (the arrow lines indicate the shoulder separation in samples with $x/y < 0,67$).

C. The SiC and metallic Te added MgB_2 bulks were tested for mechanical properties under compression with a focus on the impact dynamical ones. The SHPB tests revealed a fragmentation comparable to that for conventional ceramics such as SiC [122] and Al_2O_3 . The influence of additives was observed although their contribution is limited. Fracture mechanism was assessed within different theoretical models. The Glenn-Chudnovsky model [131] fits the best our experimental data.

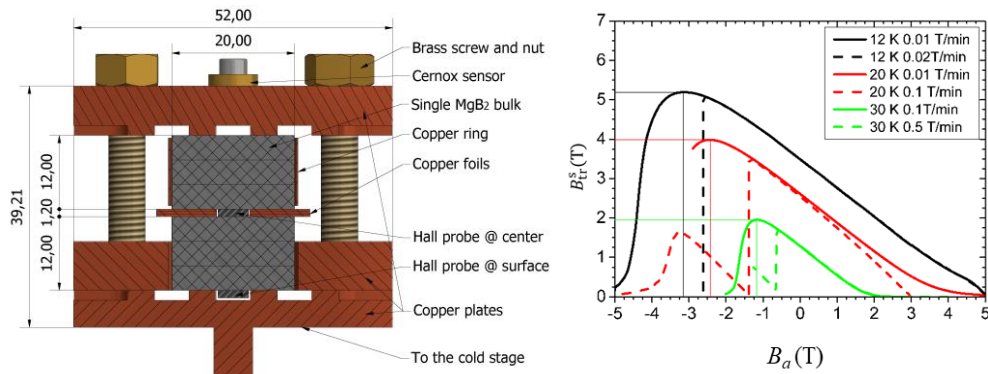


Compressive strength against strain rate for MgB_2 and other engineering ceramics.

In Section 3.1.2, $\text{Ge}_2\text{C}_6\text{H}_{10}\text{O}_7$ (A.) [A4], Te and BN-cubic (BNc) (B.) [A5] added MgB_2 bulks were obtained and investigated.

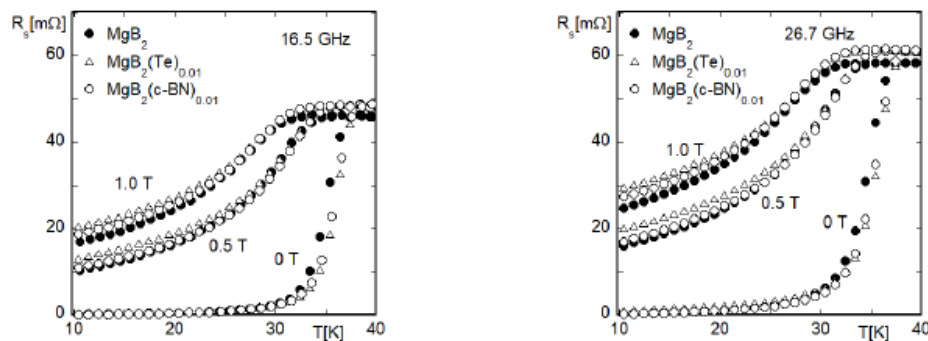
A. Six bulk discs of $\text{Ge}_2\text{C}_6\text{H}_{10}\text{O}_7$ -added MgB_2 were produced by Spark Plasma Sintering for fixed processing parameters. The samples show a good reproducibility of the process with a relatively small scattering of the superconducting properties. The capacity of these discs to trap an applied magnetic field (B_a) when assembled into a cylinder was demonstrated. The maximum trapped magnetic field (B_{tr}^S) of the compound magnet was of 5,19 T at 12 K and

3,98 T at 20 K. It is considered that a minimum magnetic field of 3 T is sufficient for practical applications.



The assembly of the compound magnet. The surface trapped magnetic field B_{tr}^s of the MgB_2 compound magnet.

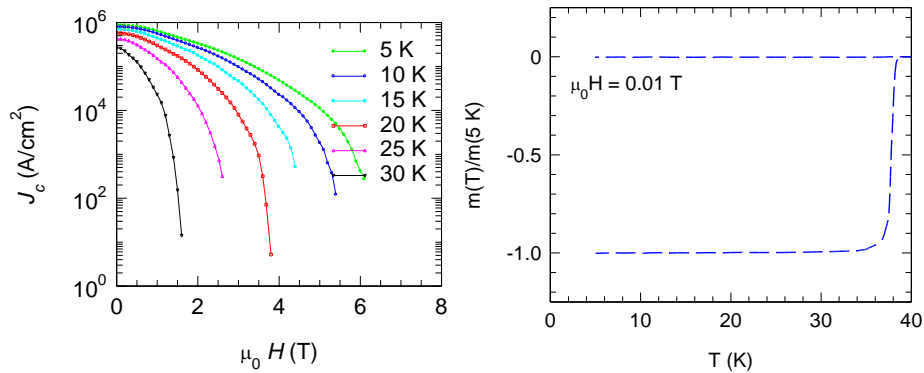
B. Dense bulks of Te and BN-cubic (BNc) added MgB_2 were investigated in a microwave environment. A dielectric resonator with a frequency of 16,5 GHz and 26,7 GHz was used. Measurements of surface resistance (R_s) were performed in a magnetic field of {0, 0,5, 1} T. The influence of additives needs higher magnetic fields to be observed. When compared with Nb_3Sn [154], MgB_2 can perform better at lower frequencies.



Surface resistance R_s vs. temperature in the 16,5 – 26,7 GHz range of the MgB_2 bulk samples.

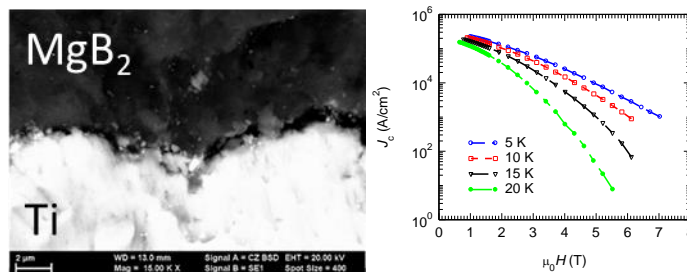
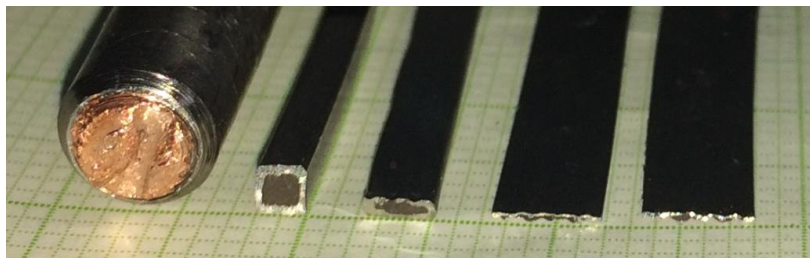
In Section 3.1.3, Fe-sheat (A.) [A6] and Ti-sheat (B.) [P1] tapes of MgB_2 are obtained by powder-in-tube technique and Spark Plasma Sintering and they are investigated.

A. The optimum temperature of sintering of MgB_2 bulks is 1150 °C [83]. In the case of wires and tapes of MgB_2 in Fe-sheat, at this sintering temperature iron melts and the integrity of the tape is lost. Therefore, a lower sintering temperature of 1050 °C was successfully used. As prepared tape was characterized from the viewpoint of superconducting properties and it was found that it has potential for application.



The critical current density J_c vs. $\mu_0 H$ at 5 – 35 K and superconducting transition for the Fe-sheath MgB₂ tapes.

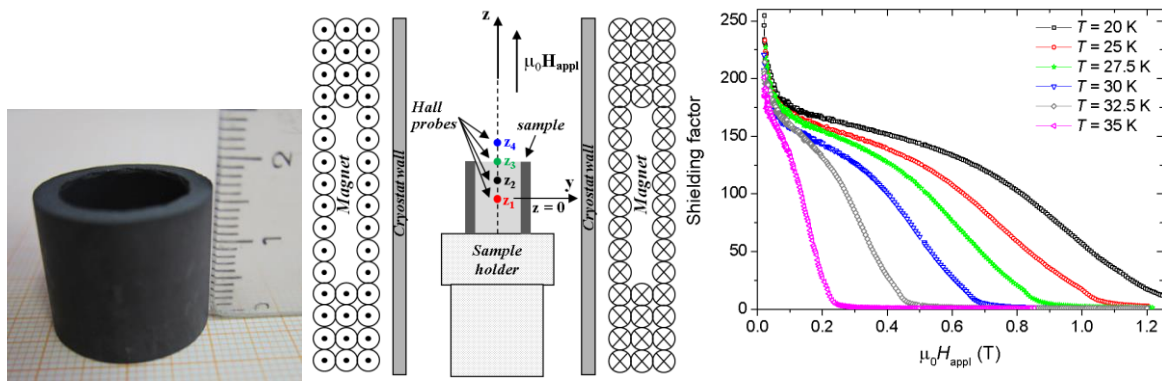
B. Tapes of MgB₂ in Ti-sheath were successfully sintered at the optimum temperature of 1150 °C. Interdiffusion between MgB₂ and Ti was limited. The superconducting properties are similar to a bulk sintered sample.



Wire and tapes of Ti-sheath MgB₂. SEM image (in backscattering mode) showing the separated Ti-sheath and MgB₂ core. Critical current density J_c vs. $\mu_0 H$ at 5 – 20 K.

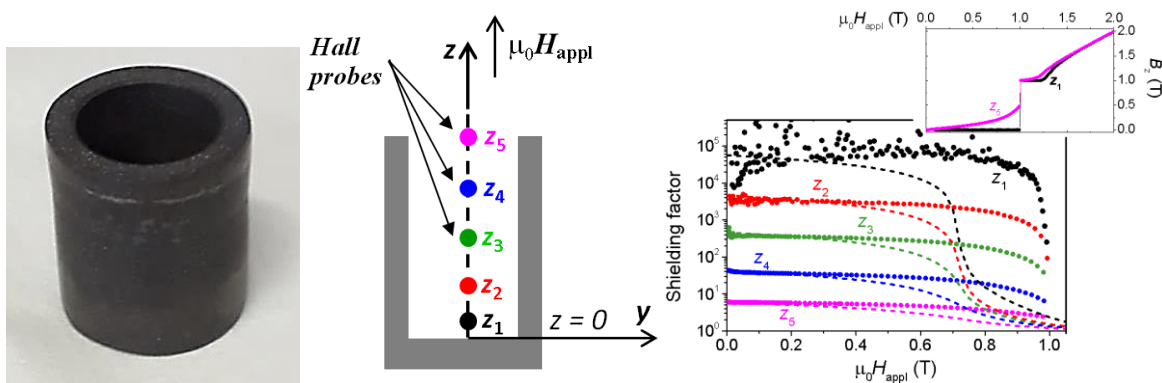
In Section 3.1.4, MgB₂ cylinder bulks added with hexagonal-BN (BNh) were obtained by Spark Plasma Sintering. The amount of BNh was so that the composite becomes machinable by chipping. Cylinders were machined to obtain different shapes (see A. [A7] and B. [A8]) that were tested for magnetic shielding properties.

A. A tube of BNh added MgB₂ ceramic cylinder was obtained by Spark Plasma Sintering and was processed by chipping on a lathe machine. The magnetic shielding factor for the axial configuration attains a shielding factor value over 175 at an applied magnetic field of 0,1 T and temperature of 20 K.



The MgB₂ tube and axial measurement position. The shielding factors with the applied magnetic field at different temperatures.

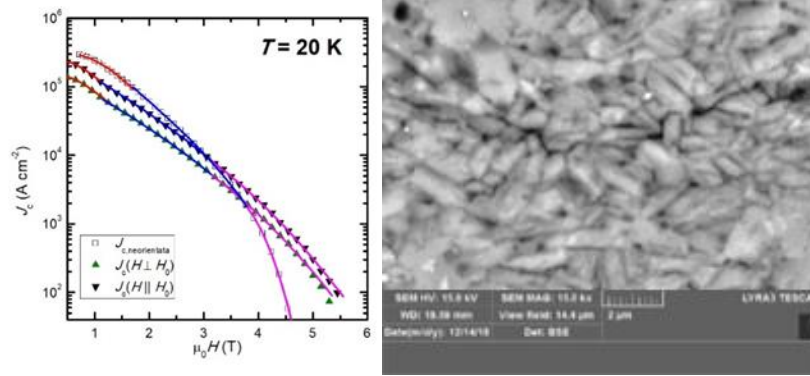
B. A tube with a cap from MgB₂ added with BNh was obtained by the same technology to that presented in subsection A. The magnetic shielding factor for the axial configuration has a much higher shielding factor value of 10⁴ at an applied magnetic field of 1 T and temperature of 20 K.



The MgB₂ cup and axial measurement position. The shielding factors with the applied magnetic field at 20 K.

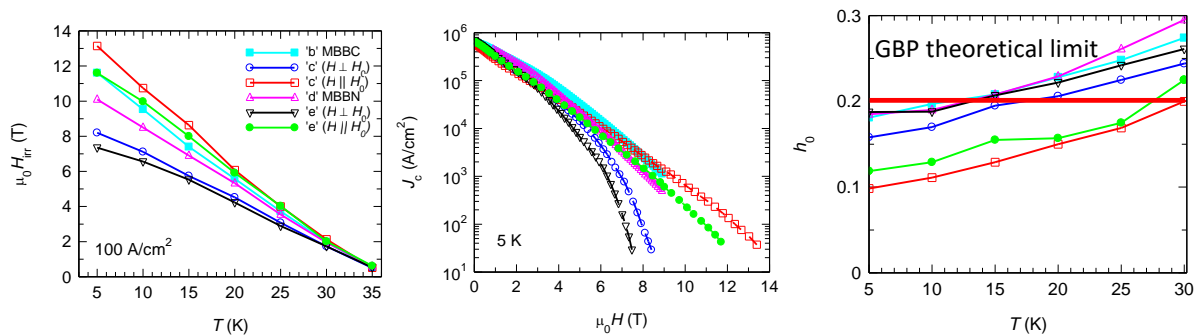
In Section 3.1.5, partially textured MgB₂ (A.) [A9] and MgB₂ added with B₄C or cubic BN (BNc) (B.) [A10] bulk samples were obtained by slip casting under high magnetic field ($H_0 = 12$ T) and Spark Plasma Sintering. Samples were characterized for an applied magnetic field parallel and perpendicular to the surface of the sintered disc.

A. The slipcasted green body shows small orientation that is improved 5,5 times after Spark Plasma Sintering. The anisotropy of $J_c(H)$ and $f_p(h)$ was revealed. The pinning force related parameters p and q from the scaling law formula $f_p = A \cdot h^p (1 - h)^q$ [23] take abnormal values when compared with theoretical ones. This result suggests that the analysis methods of the pinning force in MgB₂ need improvement.



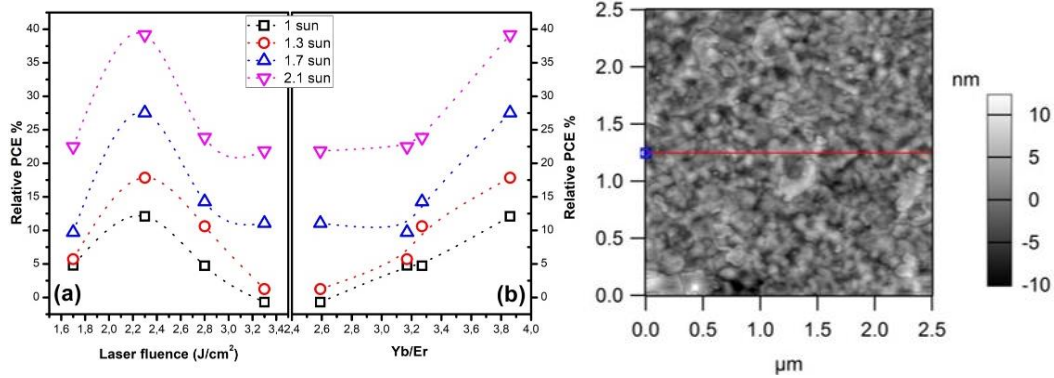
Critical current density J_c vs. $\mu_0 H$ for $H \parallel H_0$ and $H \perp H_0$ at 20 K. SEM image on the cross-section of the textured MgB₂ sample.

B. Partially textured samples of MgB₂ added with B₄C or BNC were fabricated by Spark Plasma Sintering. The orientation and additives have a synergetic effect on the microstructure development. The irreversibility field H_{irr} and critical current density J_c recorded a maximum for $H \parallel H_0$ direction. As in the previous subsection A. the pinning force related parameters, e.g. h_0 ($h_0 = h(f_p = 1)$, where $h = H/H_{\text{irr}}$) are outside of the theoretical range ($h_0 = 0,2$ for pinning on grain boundaries and $h_0 = 0,33$ for pinning on point defects [23]).



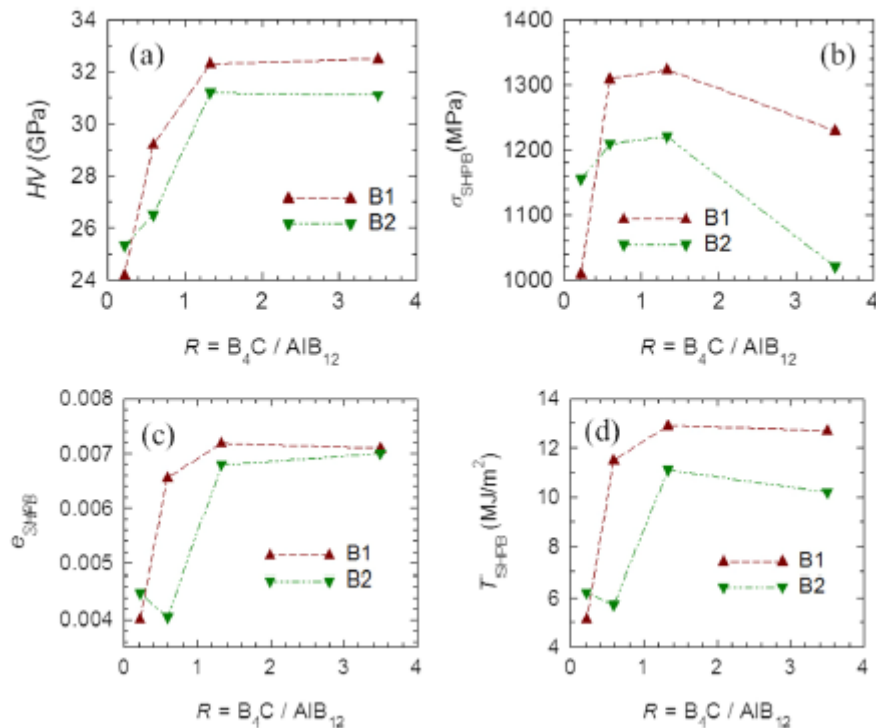
Irreversibility field $\mu_0 H_{\text{irr}}$ vs temperature, critical current density J_c vs. $\mu_0 H$ and h_0 vs. temperature for different measurement directions ($H \parallel H_0$ and $H \perp H_0$). Red line indicates the theoretical limit value of h_0 for GBP.

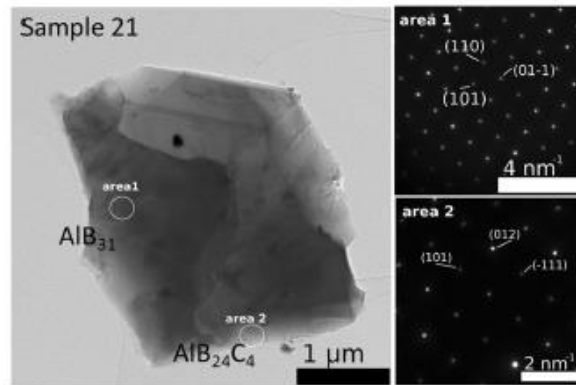
In Section 3.2.1. Yb and Er doped CeO₂ thin films were obtained at different fluences (1,7 – 3,8 J/cm²) by Pulsed Laser Deposition [A11]. We selected the rare earths ratio Yb:Er = 4:1 and a bulk target was prepared from a mixture of CeO₂, Yb₂O₃ and Er₂O₃ powders [40]. The composition, thickness and morphology of the thin films are influenced by the laser fluence. Thin films deposited at intermediate fluence (2,3 J/cm²) showed the best optical properties. The films were also grown on silicon solar cells for the optimum fluence (2,3 J/cm²). The modified cells have shown a power conversion efficiency (PCE) of 12,1 % and 39,2 % under 1 sun and 2,1 suns illumination. The upconversion process registered a relative external quantum efficiency (relative EQE) of 8,2 % when excited with a 980 nm laser diode.



The relative PCE dependence on the laser fluence (a) and on Yb/Er elemental ratio measured at different solar simulator incident powers. AFM image of the 2.3 J/cm² deposited thin film on a solar cell.

In Section 3.3.1. Dense bulk samples of Al-B-C composites were obtained by Spark Plasma Sintering for different compositions [a(80 B₄C + 20 B) + b(90 AlB₁₂ + 10 B)], a = 20, 40, 60, 80; b = 80, 60, 40, 20 ($r = B_4C/\alpha-AlB_{12} = 3,5, 1,33, 0,59, 0,22$) from mixtures of B₄C, α -AlB₁₂ and B (amorphous and crystalline) powders [A12]. The best static and dynamic mechanical properties ($HV = 32.4$ GPa, $\sigma_{SHPB} = 1323$ MPa, $e_{SHPB} = 0.0072$, $T_{SHPB} = 12.9$ MJ/m²) were recorded for the sample with $r = B_4C/\alpha-AlB_{12} = 1,33$. This sample has the highest amount of AlB₂₄C₄ phase. These results are in agreement with the theoretical predictions that the phase AlB₂₄C₄ [55] with the highest packing degree of the icosahedral B₁₂ units among all the B₁₂-containing phases in the Al-B-C system should have the best impact mechanical properties.





Vickers hardness (a) and dynamic impact parameters (c-d) of the Al-B-C samples. TEM and SAED images of the sample with $r = \text{B}_4\text{C}/\alpha\text{-AlB}_{12} = 1,33$.

CONCLUSIONS

MgB₂ composite bulk superconductors, Yb/Er CeO₂ rare earth thin film luminescent materials and Al-B-C structural composites were successfully obtained.

The introduction of different additives (In/Ga-H₂₁InO₆, SiC-Te, Ho₂O₃-Te) into MgB₂ matrix improved the superconducting and mechanical properties of the composite.

A compound magnet composed of 6 dense samples of Ge₂C₆H₁₀O₇ added MgB₂ attained a high trapped magnetic field (B_{tr}^s) of 5,19 T at 12 K and 3,98 T at 20 K.

Dense discs of pure and B₄C or Te added MgB₂ were tested and showed sensitivity to low and high frequencies microwaves, showing the possibility to detect signals from the cosmic rays (dark matter).

Fe-sheat and Ti-sheat MgB₂ powder-in-tube tapes were successfully obtained by SPS at 1050 and 1150 °C. The optimum sintering temperature of 1150 °C (for MgB₂ bulks) can be applied only for the Ti-sheat MgB₂ tape. The superconducting properties were similar to those of a bulk sample.

Cylinders of BNh added MgB₂ were obtained by SPS. The addition was introduced to allow mechanical processing into different shapes. A tube and a cup were fabricated by chipping on a lathe machine. These shapes were tested for electromagnetic shielding applications and showed shielding factors of SF = 175 (tube) at an applied magnetic field of 0,1 T and temperature of 20 K and SF = 10⁴ (cup) at an applied magnetic field of 1 T and temperature of 20 K.

Partially textured pristine MgB₂ and B₄C or BNc added MgB₂ bulks were obtained by slipcasting in high magnetic (12 T) field and SPS. The samples showed anisotropy of the superconducting properties with a maximum for $H \parallel H_0$ direction.

Yb and Er doped CeO₂ thin films were obtained by PLD. The intermediate fluence of about 2,3 J/cm² showed the best optical properties with the lowest surface roughness and spherical morphology. The thin film deposited on a silicon solar cell registred a maximum in power conversion efficiency (*PCE*) of 12,1 % and 39,2 % under 1 sun and 2,1 suns illumination.

Dense sample of Al-B-C composite obtained with SPS by mixing the precursor powders (B₄C, α-AlB₁₂ and B) with the fixed composition of 60(80 B₄C + 20 B) + 40(90 AlB₁₂ + 10 B), $r = B_4C/\alpha-AlB_{12} = 1,33$, presented the best static and dynamic mechanical properties.

PERSONAL CONTRIBUTIONS – ORIGINALITY

Results obtained are presented in Chapter 3 of the thesis and contributions of the student are as follows:

1. Development of MgB₂ superconductors

1.1. Bulks

Different additives were used to improve the superconducting properties of MgB₂.

Textured dense samples of MgB₂ were obtained for the first time.

Shaped forms of MgB₂ were obtained for magnetic shielding applications.

1.2. Tapes

Fe-sheat and Ti-sheat MgB₂ tapes were obtained by SPS. Correlation between processing and superconducting parameters were investigated.

2. Development of Yb/Er doped CeO₂ luminescent materials

Yb/Er doped CeO₂ thin films were fabricated by PLD. Efficient optical conversion was confirmed by the improvements of the PCE of the solar cells covered by the thin films.

3. Development of Al-B-C composite

It was demonstrated that obtaining the AlB₁₂C₂ phase as the major one in a Al-B-C composite leads to best static and dynamic mechanical properties.

Contributions to the *state of the art*

Additions of C₁₅H₂₁InO₆ and C₁₅H₂₁GaO₆ to MgB₂ were used for the first time.

The control of microstructural details by adding Te and H₂O₃ to MgB₂ was demonstrated.

A study on dynamic mechanical impact properties of pure MgB₂ and SiC-Te added MgB₂ composites was performed for the first time.

It was demonstrated that a compound magnet composed of 6 discs of Ge₂C₆H₁₀O₇ added MgB₂ can achieve a high trapped magnetic field of over 5 T.

Textured bulk samples of pure MgB₂ and B₄C or BNc added MgB₂ were obtained and investigated for the first time.

The possibility to fabricate complex shapes of BNh added MgB₂ with record magnetic shielding properties was explored for electromagnetic shielding applications.

PhD.Student, Mihai-Alexandru Grigoroscuta

Boron and rare earth based materials for energy applications

Short Fe and Ti-sheath powder-in-tube tapes of MgB_2 were obtained by SPS and investigated for superconducting properties.

Thin films of Yb/Er doped CeO_2 prove to be efficient in conversion of the solar spectrum. When deposited on a silicon solar cell, the thin film has shown significant improvement in the power conversion efficiency (PCE). This effect was studied for the first time on solar cells.

High amount of $\text{AlB}_{12}\text{C}_2$ phase in composite samples from the Al-B-C system were obtained and studied for mechanical applications.

PUBLISHED PAPERS

A1. Enhanced critical current density at high magnetic fields in MgB₂ with Ga/In acetylacetonate processed by spark plasma sintering, D. Batalu, G. Aldica, M. Burdusel, **M. Grigoroșcuta**, I. Pasuk, A. Kuncser, A.M. Ionescu, P. Badica, Journal of Materials Research and Technology 9 (2020) 3724-3733. (<https://doi.org/10.1016/j.jmrt.2020.01.109>).

A2. Ch. 11 Control of the Critical Current Density Through Microstructural Design by Ho₂O₃ and Te Co-addition into MgB₂ Processed by Ex Situ Spark Plasma Sintering, P. Badica, G. Aldica, M. Burdusel, **M. Grigoroșcuta**, A. M. Ionescu, V. Sandu, S. Popa, M. Enculescu, I. Pasuk, A. Kuncser, in Superconductivity, From Materials Science to Practical Applications, (Eds. Mele P. et al.), (2020) 303-324. ISBN 978-3-030-23302-0. (<https://doi.org/10.1007/978-3-030-23303-7>).

A3. Compressive properties of pristine and SiC-Te-added MgB₂ powders, green compacts and spark-plasma-sintered bulks, P. Badica, D. Batalu, M. Burdusel, **M.A. Grigoroșcuta**, Gh.V. Aldica, M. Enculescu, R.A. Gabor, Z. Wang, R. Huang, P. Li, Ceramics International 44 (2018) 10181-10191. (<https://doi.org/10.1016/j.ceramint.2018.03.008>).

A4. Reproducibility of small Ge₂C₆H₁₀O₇-added MgB₂ bulks fabricated by ex situ Spark Plasma Sintering used in compound bulk magnets with a trapped magnetic field above 5 T, P. Badica, G. Aldica, **M. A. Grigoroșcuta**, M. Burdusel, I. Pasuk, D. Batalu, K. Berger, A. Koblishka-Veneva, M. R. Koblishka, Scientific Reports 10 (2020) 10538. (<https://doi.org/10.1038/s41598-020-67463-y>).

A5. Microwave investigation of pinning in Te- and cubic-BN- added MgB₂, A. Alimenti, K. Torokhtii, **M. Grigoroșcuta**, P. Badica, A. Crisan, E. Silva, N. Pompeo, Journal of Physics: Conference Series 1559 (2020) 012039. (<https://doi.org/10.1088/1742-6596/1559/1/012039>).

A6. Powder-in-tube tapes of MgB₂ in Fe-sheath processed by ex-situ Spark Plasma Sintering, M. Burdusel, A.M. Ionescu, **M. Grigoroșcuta**, D. Batalu, M. Enculescu, S. Popa, V. Mihalache, G. Aldica, P. Badica, UPB Scientific Bulletin Series C-Electrical Engineering and Computer Science 79 (2017) 155-172. (ISSN 1454-2331).

A7. Passive magnetic shielding by machinable MgB₂ bulks: measurements and numerical simulations, L. Gozzelino, R. Gerbaldo, G. Ghigo, F. Laviano, D. Torsello, V. Bonino, M. Truccato, D. Batalu, **M. Grigoroșcuta**, M. Burdusel, G. Aldica, P. Badica, Superconductor Science and Technology 32 (2019) 034004-9pp. (<https://doi.org/10.1088/1361-6668/aaf99e>).

A8. High magnetic shielding properties of an MgB₂ cup obtained by machining a spark-plasma-sintered bulk cylinder, L. Gozzelino, R. Gerbaldo, G. Ghigo, D. Torsello, V. Bonino, M. Truccato, **M. A. Grigoroșcuta**, M. Burdusel, Gh. V. Aldica, V. Sandu, I. Pasuk and P. Badica, Supercond. Sci. Technol. 33 (2020) 044018. (<https://doi.org/10.1088/1361-6668/ab7846>).

PhD.Student, Mihai-Alexandru Grigoroscuta

Boron and rare earth based materials for energy applications

A9. Superconducting MgB₂ textured bulk obtained by ex-situ Spark Plasma Sintering from green compacts processed by slip casting under 12 T magnetic field, **M. A. Grigoroscuta**, V. Sandu, A. Kuncser, I. Pasuk, G. Aldica, T. Suzuki, O. Vasykiv, P. Badica, Superconductor Science and Technology 32 (2019) 125001. (<https://doi.org/10.1088/1361-6668/ab4620>).

A10. Partially oriented MgB₂ superconducting bulks with addition of B₄C and cubic BN obtained by slip casting under high magnetic field and spark plasma sintering, **M. Grigoroscuta**, Gh. Aldica, I. Pasuk, M. Burdusel, V. Sandu, A. Kuncser, T. Suzuki, O. Vasykiv, P. Badica, Materials Research Bulletin 134 (2021) 111103. (<https://doi.org/10.1016/j.materresbull.2020.111103>).

A11. Enhanced near-infrared response of a silicon solar cell by using an up-conversion phosphor film of Yb/Er – co-doped CeO₂, **M. Grigoroscuta**, M. Secu, L. Trupina, M. Enculescu, C. Besleaga, I. Pintilie, P. Badica, Solar Energy vol. 171, pp. 40–46 (2018). (<https://doi.org/10.1016/j.solener.2018.06.057>).

A12. Bulks of Al-B-C obtained by reactively spark plasma sintering and impact properties by Split Hopkinson Pressure Bar”, O. Vasykiv, H. Borodianska, D. Demirskyi, P. Li, T. S. Suzuki, **M. A. Grigoroscuta**, I. Pasuk, A. Kuncser and P. Badica, Scientific Reports 9 (2019) 19484. (<https://doi.org/10.1038/s41598-019-55888-z>).

Patent request (OSIM):

P1. Processing superconductor strip or wire comprising magnesium diboride-based core, involves performing plastic deformation and intense electric field-assisted sintering, immersing strip/wire under vacuum and heating strip/wire, **M. A. Grigoroscuta**, M. Burdusel, G. V. Aldica, P. Badica, RO133106-A2 (2017).

REFERENCES

- [1] *T.M. Letcher*, Chapter 1 - Introduction with a Focus on Atmospheric Carbon Dioxide and Climate Change, *Future Energy (Second Edition): Improved, Sustainable and Clean Options for our Planet*, Elsevier, 2014, pp. 3-16. (<https://doi.org/10.1016/B978-0-08-099424-6.00001-6>).
- [4] *G. Bhardwaj, M. Allen, O. Sarmad*, Hitting 1.5°C: The Stark Climate Choices for Governments, INTERVIEW on Paris Agreement, 2018. https://www.chathamhouse.org/expert/comment/hitting-1.5-c-stark-climate-choices-governments?gclid=Cj0KCCQjwhZr1BRCLARIsALjRVQOrqOgUd4_pZbtqFz3Kma18ROY8kSndP50_o-E8urXpFjyQS6xoboYaAk94EALw_wcB# Accesat la 21.02.2021).
- [8] *SOLARGIS*, Solar resource maps of Europe: Global Horizontal Irradiance Map of Europe, 2019. (<https://solargis.com/maps-and-gis-data/download/europe>. Accesat la 21.02.2021).
- [10] *A. Betz*, Introduction to the Theory of Flow Machines **1st Edition**, 1966, (D. G. Randall, Trans.) Oxford: Pergamon Press., Elsevier (<https://doi.org/10.1016/C2013-0-05426-6>).
- [12] *A. Botterud, T. Levin, V. Koritarov*, Pumped storage hydropower: Benefits for grid reliability and integration of variable renewable energy. Technical Report ANL/DIS-14/10 106380, 2014. (<https://doi.org/10.2172/1165460>).
- [14] *NIST Center for Neutron Research*, Neutron Scattering Lengths and Cross Sections, (<http://www.ncnr.nist.gov/resources/n-lengths/>. Accesat la 21.02.2021).
- [23] *D. Dew-Hughes*, Flux pinning mechanisms in type II superconductors, *Philos. Mag.* **vol. 30**, 1974, 293-305. (<https://doi.org/10.1080/14786439808206556>).
- [24] *M. Eisterer*, Magnetic properties and critical currents of MgB₂, *Supercond. Sci. Technol.* **vol. 20**, 2007, R47-73. (<https://doi.org/10.1088/0953-2048/20/12/R01>).
- [40] *F. Vetrone, J.-C. Boyer, J.A. Capobianco, A. Speghini, M. Bettinelli*, Effect of Yb³⁺ Codoping on the Upconversion Emission in Nanocrystalline Y₂O₃:Er³⁺, *J. Phys. Chem.* **B vol. 107**, 2003, 1107-1112. (<https://doi.org/10.1021/jp0218692>).
- [55] *A. Koroglu, D.T. Thomson*, In vacuo production of α-AlB₁₂, Ca₄AlB₂₄, AlB₁₂C₂ and Al₃B₄₈C₂ powders, *J. Eur. Ceram. Soc.* **vol. 32**, 2012, 3501–3507. (<https://doi.org/10.1016/j.jeurceramsoc.2012.04.032>).
- [83] *G. Aldica, D. Batalu, S. Popa, I. Ivan, P. Nita, Y. Sakka, O. Vasylykiv, L. Miu, I. Pasuk, P. Badica*, Spark plasma sintering of MgB₂ in the two-temperature route, *Physica C*, **vol. 477**, 2012, pp. 43-50. (<https://doi.org/10.1016/j.physc.2012.01.023>).

[122] *H. Wang, K.T. Ramesh*, Dynamic strength and fragmentation of hot-pressed silicon carbide under uniaxial compression, *Acta Mater.* **vol. 52**, 2004, pp. 355. (<https://doi.org/10.1016/j.actamat.2003.09.036>).

[131] *L.A. Glenn, A. Chudnovsky*, Strain-energy effects on dynamic fragmentation, *J. Appl. Phys.* **vol. 59**, 1986, pp. 1379. (<https://doi.org/10.1063/1.336532>).

[154] *A. Alimenti, N. Pompeo, K. Torokhtii, T. Spina, R. Flukiger, L. Muzzi, E. Silva*, Surface Impedance Measurements on Nb₃Sn in High Magnetic Fields, *IEEE Trans. Appl. Supercond.* **vol. 29**, 2019, pp. 1-4. (<https://doi.org/10.1109/TASC.2019.2892584>).